QUEST Technical Report No. 650

IN SITU COMPOSITES IN THE ALUMINUM NITRIDE-ALUMINA SYSTEM

E. Savrun

April 1995

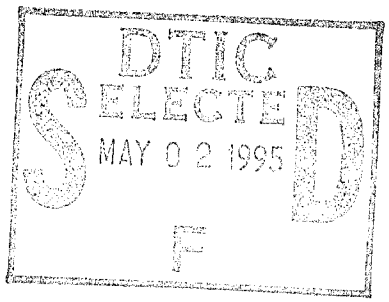

Prepared for

OFFICE OF NAVAL RESEARCH

Under Contract No. N00014-94-C-0263

Approved for public release; SBIR report, distribution unlimited.
Research supported by the Ballistic Missile Defense/Innovative Science and Technology and managed by the Office of Naval Research.

QUEST INTEGRATED, INC.
21414 - 68th Avenue South
Kent, Washington 98032
(206) 872-9500

REPORT DOCUMENTATION PAGE

Form Approved
OMB No 0704-0188

1. AGENCY USE ONLY (Leave blank)	2. REPORT DATE	3. REPORT TYPE AND DATES COVERED
	April 1995	Final Report, 19 Sept. 94 - 19 April 95

4. TITLE AND SUBTITLE
In Situ Composites in the Aluminum Nitride-Alumina System

5. FUNDING NUMBERS
N00014-94-C-0263

6. AUTHOR(S)
Ender Savrun

7. PERFORMING ORGANIZATION NAME(S) AND ADDRESS(ES)
QUEST Integrated, Inc.
21414 68th Avenue South
Kent, WA 98032

8. PERFORMING ORGANIZATION REPORT NUMBER
QUEST TR-650

9. SPONSORING MONITORING AGENCY NAME(S) AND ADDRESS(ES)
Office of Naval Research
800 North Quincy Street
Arlington, VA 22217-5660

10. SPONSORING MONITORING AGENCY REPORT NUMBER

11. SUPPLEMENTARY NOTES

12a. DISTRIBUTION AVAILABILITY STATEMENT
Approved for public release; ~~SBIR report~~, distribution unlimited. Research supported by the Ballistic Missile Defense/Innovative Science and Technology and managed by the Office of Naval Research.

12b. DISTRIBUTION CODE

13. ABSTRACT (Maximum 200 words)

An attempt was made to produce in situ composites in an aluminum nitride-alumina system via pressureless reaction sintering. Different aluminum nitride-alumina compositions were prepared and fired at temperatures between 1900°C and 2200°C. Phase compositions were determined by x-ray diffraction, and microstructure development was evaluated by scanning electron microscopy. Elongated grains in an equiaxed matrix were achieved. However, the expected improvement in mechanical properties was offset by excessive grain growth and porosity. The high mobility of grain boundaries causes abnormal growth and pore entrapment without full densification. Suggestions for further work are offered to remedy the problems.

[illegible]

14. SUBJECT TERMS	15. NUMBER OF PAGES
Aluminum Nitride, Aluminum Oxide, Ceramics, In Situ Composites, Liquid-Phase Sintering, Polymorphous Transformation, Self-Reinforced Microstructure	29
	16. PRICE CODE

17. SECURITY CLASSIFICATION OF REPORT	18. SECURITY CLASSIFICATION OF THIS PAGE	19. SECURITY CLASSIFICATION OF ABSTRACT	20. LIMITATION OF ABSTRACT
Unclassified	Unclassified	Unclassified	Unlimited

TABLE OF CONTENTS

LIST OF FIGURES AND TABLES

1. INTRODUCTION

In this Phase I Small Business Innovation Research (SBIR) project, QUEST Integrated, Inc., has conducted research to develop in situ ceramic composites in the aluminum nitride-alumina system. This final report documents the Phase I effort.

1.1 Statement of Problem and Opportunity

Microstructures containing a specific proportion of grains with a distinctive morphological anisotropy can be formed in certain ceramic materials during liquid-phase sintering without the use of initial crystals with anisotropic forms, i.e., whiskers. The sintering of these materials is accompanied by polymorphous transformations. The grains of resulting phases in subsequent growth, which assume an elongated, whisker-like (acicular) shape, can act as reinforcements in the microstructure. We refer to materials with this type of microstructure as self-reinforced materials or in situ composites. In situ composites can overcome the problems common in conventional whisker-reinforced composites. Problems associated with manufacturing whisker-reinforced composites include the high cost of whiskers; potential health hazards in their handling; processing difficulties, e.g., uniform dispersion; and high processing costs. Such materials based on silicon nitride show an increase in fracture toughness and bending strength at room temperature; however, the presence of glassy grain-boundary layers in Si_3N_4 results in poor mechanical properties and low creep resistance at high temperatures.

The aluminum nitride (AlN) - alumina (Al_2O_3) system has many phases that are based on the AlN wurtzite structure and exhibits many polymorphous phase transformations resulting in plate-like (Tkachenko et al., 1992) and whisker-like grain morphologies (Corbin, 1989; Long and Foster, 1961; McCauley and Corbin, 1983; McCauley et al., 1987; Komeya and Inoue, 1971; Komeya et al., 1974; and Zangvil and Doser, 1982). Transmission electron microscopy work has shown that the grain boundaries in the AlN-Al_2O_3 system are free of any glassy phase (Zangvil and Doser, 1982). Even when SiO_2 is deliberately added, it goes into the AlN lattice and leaves grain boundaries clean (Sarikaya and Thomas, 1984, and Sarikaya et al., 1985). Therefore, in situ composites in the AlN-Al_2O_3 system are expected to have better mechanical properties and creep resistance than Si_3N_4 at high temperatures.

The AlN-Al_2O_3 system may be used to develop self-reinforced materials with excellent mechanical properties and creep resistance at high temperatures. To do so will require a complete understanding of the effects of processing variables on microstructural evolution, in particular, the effect of powder chemistry on acicular grain formation.

1.2 Objective

The objective of the Phase I program was to develop an in situ composite in the aluminum nitride-alumina system with room-temperature mechanical properties: 1000 MPa bend strength and 7-8 MPa in 1/2 fracture toughness. These values are comparable to those of self-reinforced silicon nitride but with better high-temperature properties than those of silicon nitride.

1.3 Aluminum Nitride - Aluminum Oxide System

The first phase diagram for this system was reported by Lejus (1964). Six phases were identified, including a phase designated 'X' that encompassed all compositions for the polytype phases. Figure 1

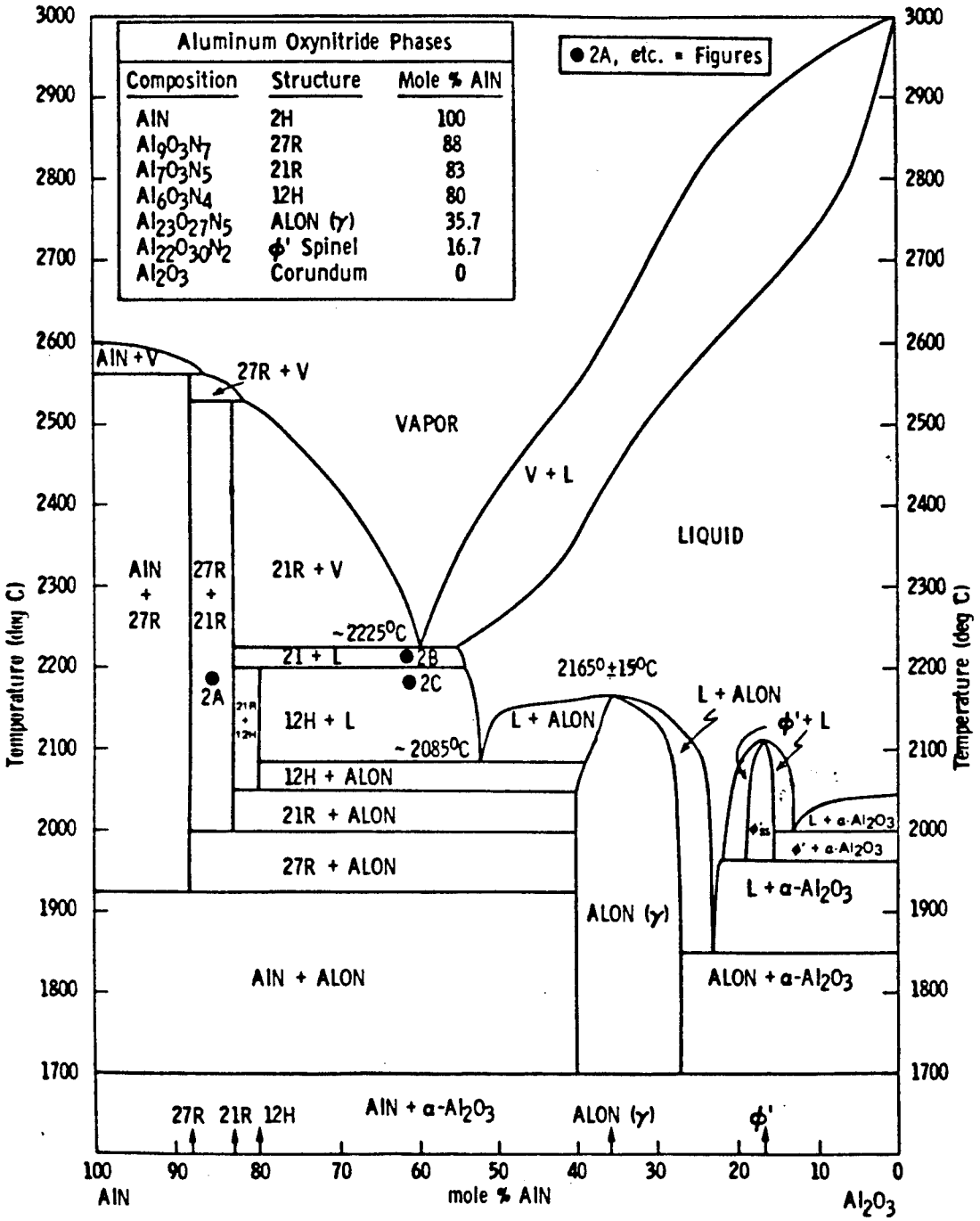

Figure 1. AlN-Al_2O_3 Phase Diagram (McCauley and Corbin, 1983)

shows the most recent phase diagram as reported by McCauley and Corbin (1983) for an atmosphere of 0.101 MPa (1 atm) N_2.

Table 1 lists 13 aluminum oxynitride phases that have been observed along with their nomenclature and composition. The phases can be separated into two groups depending on their basic crystallographic structure. One group is based on polytypes of the wurtzite structure, and the other on the spinel structure.

The phases commonly termed "aluminum nitride polytypes" are based on the AlN wurtzite structure (Jack, 1976). Since these phases are compositionally controlled, they are not true polytypes, as SiC polytypes are. Most studies on these polytype phases have been conducted in the Si-Al-O-N system. As a result, most reported information on these phases shows silicon to be present in the structure.

McCauley and Corbin (1983) and Long and Foster (1961) have observed the formation of acicular grains in the AlN-Al_2O_3 system. McCauley and Corbin implied that a polymorphous phase transformation responsible for acicular grain growth is activated by oxygen insertion into a 2H wurtzite AlN lattice.

Table 1. Aluminum Nitride Polytypes Observed in the AlN-Al_2O_3 System (Corbin, 1989)

Notation	Mole % AlN	Formula	M : X[a]	Structure
2H	100.0	AlN	1 : 1	Polytype[b]
32H	93.3	$Al_{16}O_3N_{14}$	16 : 17	Polytype
20H	88.9	$Al_{10}O_3N_8$	10 : 11	Polytype
$2H^{\delta}$	—	—	> 9 : 10	Polytype
27R	87.5	$Al_9O_3N_7$	9 : 10	Polytype
16H	85.7	$Al_8O_3N_6$	8 : 9	Polytype
21R	83.3	$Al_7O_3N_5$	7 : 8	Polytype
12H	80.0	$Al_6O_3N_4$	6 : 7	Polytype
γ-AlON	35.7	$Al_{23}O_{27}N_5$	23 : 32	Spinel
γ'-AlON	~ 21.0	$Al_{19.7}O_{29.5}N_{2.5}$	19.7 : 32	Spinel
ϕ'-AlON	16.7	$Al_{22}O_{30}N_2$	22 : 32	Spinel
δ-AlON	10.0	$Al_{19}O_{27}N$	19 : 28	Spinel
ϕ-AlON	7.1	$Al_{27}O_{39}N$	27 : 40	Monoclinic
Corundum	0.0	Al_2O_3	2 : 3	Corundum

[a]Cation (M) : anion (X) ratio

[b]Composition assumes that only Al, O, and N are present

However, transmission electron microscopy work showed the presence of silicon in the acicular grains. It has been speculated that preferential substitution of silicon impurities into an AlN lattice may be responsible for polymorphous phase transformations that lead to acicular grain growth. Neither McCauley and Corbin nor Long and Foster studied the mechanical properties of these self-reinforced materials.

Figure 2 relates the microstructures obtained by McCauley and Corbin to the phase diagram in Figure 1 (McCauley and Corbin, 1983). It is clear that in certain phase regions whisker-like (acicular) grains can be achieved in a fully dense matrix. These microstructures are expected to be self-reinforcing, thus forming in situ composites in the AlN-Al_2O_3 system.

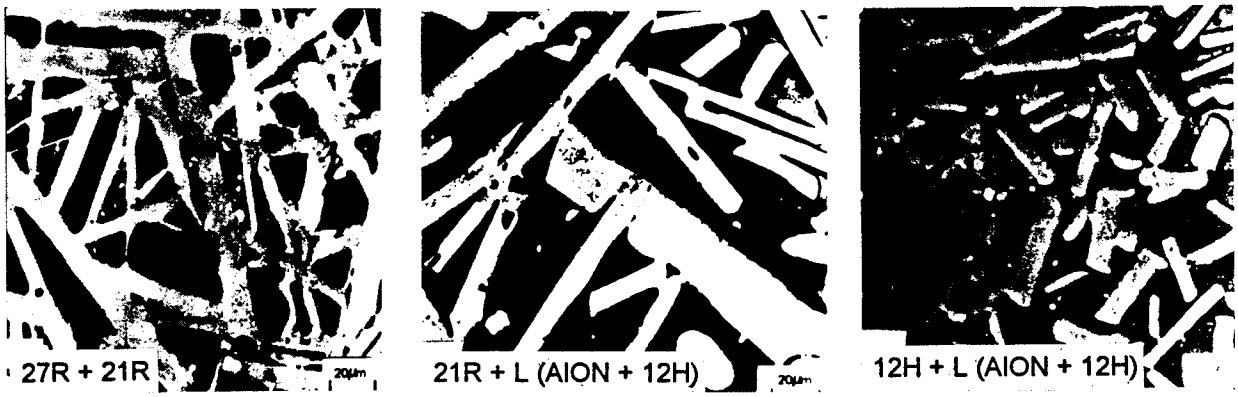

Figure 2. Self-Reinforced Microstructures in the AlN-Al_2O_3 System (McCauley and Corbin, 1983)

2. GENERAL PROGRAM DESCRIPTION

2.1 Technical Approach

The technical approach to develop an in situ composite in the aluminum nitride-alumina system included the following activities:

- Preparation of seven different compositions in the AlN-Al_2O_3 system by wet mixing and spray drying.
- Compaction of spray-dried powders.
- Binder removal and sintering of compacts.
- Microstructural evaluation.
- Characterization of mechanical properties.

The approach to the program was structured with industrial scalability in mind. The tasks were carried out in a way that is compatible with current industrial ceramic-processing practices; therefore, the process is readily scalable for commercial production.

2.2 Task Breakdown

The following tasks were performed during the proposed project: The work conducted under each task is discussed in more detail in the following sections.

Task 1: Powder Preparation

The physical and chemical properties of AlN, Al_2O_3, and Y_2O_3 powders were determined. The dispersion conditions were identified, including binder, dispersant, solvent, and mixing methods. Prepared powder slurries were granulated by spray drying for subsequent pressing operations.

Task 2: Consolidation and Binder Removal

Several 16.5-mm (0.65-in.) diameter specimens of varying thickness were pressed. A density-pressure matrix was constructed to determine the pressing pressure. Microstructures of consolidated green compacts were evaluated to determine the efficiency of the binder and the pressing process. The time, temperature, and atmosphere were defined to prevent the oxidation of AlN while avoiding the formation of residual carbon during binder removal.

Task 3: Sintering and Microstructural Evaluation

Sintering was performed in a nitrogen environment in boron nitride crucibles using a graphite element furnace. The effects of temperature and time on the density, microstructure, and phase compositions were investigated.

Task 4: Mechanical Testing

Mechanical test samples were prepared by diamond machining. Flexural strength, hardness, indentation fracture toughness, and elastic modulus were measured.

3. TASK 1: POWDER PREPARATION

3.1 Materials

Information about the materials used during the experiments is listed in Tables 2 and 3. Table 2 lists materials used throughout the program, and Table 3 lists the compositions that were studied.

Table 2. Starting Materials

Material	Source		Particle Size d_{50}, microns		Surface Area, m^2/g
Alumina	Ceralox HPA-0.5 AF		0.48		9.5
Aluminum Nitride	Dow Electronics Grade		1.64		4.59
Yttria	Rhône-Poulenc 99.99F		0.55		8.1
	C, % wt	O, % wt	Si, ppm	Ca, ppm	Fe, ppm
Alumina	--	--	19	7	9
Aluminum Nitride	0.075	1.8	81	96	23

Table 3. Compositions Studied

Sample	% wt			
	AlN	Al_2O_3	Y_2O_3	SiO_2
A	28.67	71/33	--	--
B	32.94	67.06	--	--
C	37.61	62.39	--	--
D	42.74	57.26	--	--
E	69.49	30.51	--	--
F	88.42	11.58	--	--
G	30.76	69.24	--	--
DY	41.10	55.05	3.85	--
DYS	40.90	54.80	3.82	0.48
EY	66.81	29.33	3.86	--

3.2 Dispersion

A controlled green microstructure is essential if a uniform, fully dense sintered body is desired. Good powder dispersion is the first step to a controlled green microstructure. Physical and chemical properties of the starting powders, solids loading, dispersion medium, dispersant, binder, order of addition, milling speed, and time can affect the state of dispersion.

A good binder for pressing operations should provide enough green strength to prevent parts from breaking during handling yet should be weak enough to ensure that spray-dried granules will break under applied pressure. Complete granule breakage is necessary to eliminate the large intergranular pores that can exist between unbroken granules during pressing.

An acrylic polymer (Acryloid DM55, Rohm and Haas Co.) and polyethylene glycol (PEG 3350, Union Carbide) mixture was used as a binder. A polyester/polyamine copolymer (Hypermer KD1, ICI Americas) was chosen as a dispersant. Acetone was used as the solvent.

The dispersant was dissolved in the solvent, and the powders were added to the solution to form a suspension with 5% vol solids loading. Suspensions were dispersed by sonicating with an 800-W sonic probe (Heat Systems, Sonicator 800) for 60 seconds. Dispersions were poured in graduated cylinders for sedimentation tests. Sediment and supernatant heights were checked periodically to assess the quality of dispersion.

3.3 Spray Drying

Al_2O_3-AlN mixtures were prepared by ball milling. Al_2O_3, AlN, Y_2O_3, and SiO_2 powders were mixed in dispersant acetone solution and milled in polyethylene jars with a high-purity alumina charge for 1.5 hr. The binder and plasticizer were dissolved in acetone, added to the charge, and milled for an additional 1.5 hr. The quality of dispersion was monitored by measuring viscosity with a rotary viscometer (Rheoset LV, Brookfield Engineering Labs). Solids loading was fixed at 30% vol for ease of spray drying.

Slurries were granulated by spray drying (Yamato spray dryer, GB-22 Floor Model). Spray drying parameters were as follows:

- Inlet temperature = 64°C
- Outlet temperature = 21°C
- Carrier gas (nitrogen) flow rate = 0.26 m^3/min
- Atomizer pressure = 0.8 kgf/cm^2
- Atomizer nozzle diameter = 0.5 mm

4. TASK 2: CONSOLIDATION AND BINDER REMOVAL

4.1 Pressing

Granulated powders were pressed in a steel die on a hydraulic press (Model M, Fred S. Carver, Inc.). A density-pressure matrix was constructed to optimize pressing pressure. High pressure causes high elastic springback, which in turn results in end capping and delamination. High pressure also causes immature die failure. Low pressure results in incomplete consolidation, which causes low green density.

4.2 Binder Removal

Complete binder removal is necessary because residual carbon can adversely affect densification, degrading final material properties including transparency. The rate of binder removal is also important. A fast removal rate can cause cracking, while too slow a rate can cause char formation.

Burn-out characteristics of the organics (binder + plasticizer + dispersant) were studied with thermal gravimetric analysis (Setra 1700, Astra Scientific Instruments). A sample of spray-dried powder was heated to 800°C at a rate of 5°C/min in air. Weight loss was recorded as a function of temperature. Thermal gravimetric analysis results were used to devise a binder-removal profile.

5. TASK 3: SINTERING AND MICROSTRUCTURAL EVALUATION

AlN-Al_2O_3 mixtures with and without Y_2O_3 and SiO_2 were fired in boron nitride crucibles using a graphite element furnace (ASTRO, Thermal Technologies) at temperatures from 1900°C to 2200°C for 1 hr and 6 hr. A nitrogen atmosphere with a pressure of 5 psig (34 kPa) and a flow rate of 12.75 ℓ/hr was maintained in all experiments. Specimen dimensions were measured before and after sintering to calculate the shrinkage. Sintered densities were measured via the liquid immersion technique in methyl alcohol.

Weight loss and shrinkage were determined. Detailed phase analyses were carried out using the x-ray diffraction technique to follow the phase transformation reactions. The specimens were ceramographically polished and thermally etched to study microstructural evolution. They were then cut with a low-speed diamond saw (Isomet, Buehler) and mounted in a thermoplastic resin (Transoptic, Buehler) for grinding and polishing. The grinding and rough polishing were done on a grinder with a diamond disk (Ecomet 3, Buehler). The final polishing was done with a 1-μm diamond paste. The specimens were dismounted by heating for 10 min at 140°C. They were ultrasonically cleaned in acetone, and etched in nitrogen for 1 hr at 1600°C. The specimens were mounted on aluminum stubs with colloidal graphite and lightly coated with gold-palladium alloy for examination under a scanning electron microscope. The microscope was equipped with a Robinson backscattered electron detector and an energy dispersive x-ray analyzer.

6. TASK 4: MECHANICAL TESTING

The 2.0-mm × 2.0-mm × 25.0-mm samples were machined from 50-mm-diameter and 4.0-mm-thick disks and tested in three-point bending with a 20-mm outerspan. The strengths were calculated from the simple beam theory:

$$\sigma = 3PL/bd^2 \tag{1}$$

where σ is the strength, P is the applied load, L is the beam length, b is the beam width, and d is the beam depth.

The strength data were analyzed using a two-parameter Weibull expression (Savrun, 1986). The Weibull cumulative distribution function is given by

$$F = 1 - \exp(-(\sigma/\sigma_0)^m) \tag{2}$$

where F is the probability of failure, σ is fracture strength, σ_0 is a scaling parameter, and m is the Weibull modulus. Values for F are calculated via order statistics according to:

$$F = n/N + 1 \tag{3}$$

where n is the order of the strength and N is the total number of data points.

Insertion of Equation (3) into Equation (2) and a double logarithmic transformation gives

$$\ln \ln 1/1-F = m \ln \sigma - m \ln \sigma_0 \tag{4}$$

A least-squares linear regression analysis is used to calculate the Weibull parameters σ_0 and m in Equation (4). A correlation coefficient, R, is also calculated to determine the goodness-of-fit of the data to the two-parameter Weibull model.

Hardness and fracture toughness measurements were performed on polished samples via Vickers indentation techniques. In the hardness test, a load of 500 grams was used to prevent the cracking of the sample. Hardness values were calculated from

$$H = 0.47\, P/a^2. \tag{5}$$

where H is the hardness and a is half the indentation length. Fracture toughness measurements were made under a 10-kg load to induce cracking. The fracture toughness, K_c, was calculated according to Anstis et al. (1981):

$$K_c = 0.016\, (E/H)^{1/2}\, (P/C_0^{3/2}) \tag{6}$$

where E is the elastic modulus and C_0 is the radical crack length

The elastic modulus was measured by the resonant frequency method using a commercial instrument (Grindo-Sonic, St. Louis, MO). Sample bars used in flexural strength tests were used in elastic modulus measurements. Tests were carried out according to ASTM C623 test methods. The elastic modulus was calculated from

$$E = CWf^2 \tag{7}$$

where C is a function of the sample geometry, W is the sample weight, and f is fundamental flexural resonant frequency.

7. RESULTS AND DISCUSSION

7.1 Dispersion

Hypermer KD1 dispersant worked well for codispersion of AlN and Al_2O_3 in acetone. Figure 3 gives the changes in viscosity with milling time. The viscosity changed significantly with milling time for 1.0% wt KD1, suggesting we need to add more dispersant. The addition of 1.5% wt KD1 reduced the slurry viscosity significantly and decreased the milling time required to reach a fully dispersed state to 3 hours. It is possible to decrease the milling time by increasing the KD1 to 2.0% wt, but this will be tested in Phase II. The observed shear thinning behavior suggests all dispersions were partially flocculated, but they were considered acceptable for our purposes.

The stability of the dispersion was assessed using a sedimentation technique. All dispersions were stable. No sedimentation was observed after 24 hr.

7.2 Spray Drying and Pressing

Spray drying did not present any problems. The granule size was determined by scanning electron microscopy (SEM) and found to be 15 to 85 μm. This is slightly smaller than the standard range of 40 to 105 μm found in the industry.

From the pressure-density matrix, given in Table 4, 206 MPa (30 ksi) was selected as the optimum pressing pressure. Pressures higher than 206 MPa did not improve the green density. Furthermore, pressures higher than 206 MPa are not practical for industrial applications, because they can cause pressing defects, such as end capping and delamination, and excessive tool wear.

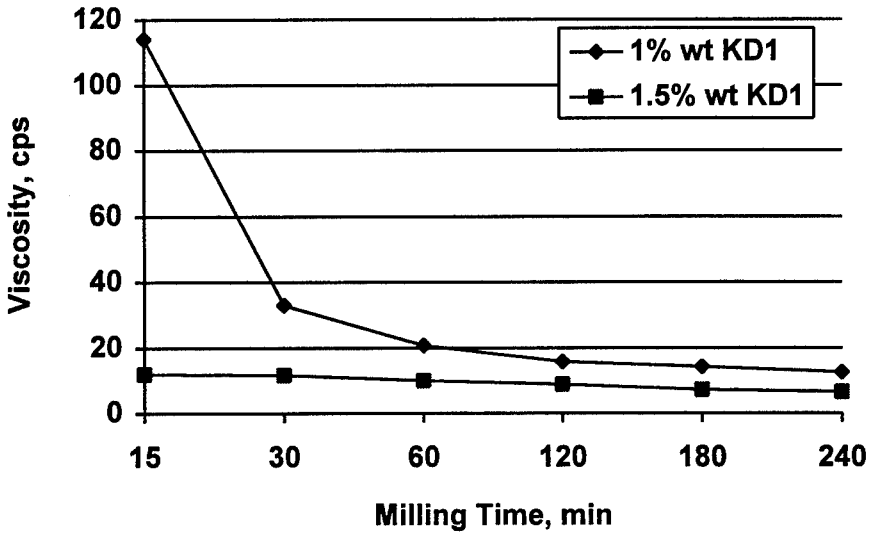

Figure 3. Milling Curve for AlN-Al_2O_3/Acetone Suspensions with Different KD1 Additions

Table 4. Pressure-Density Matrix

Pressure, MPa (ksi)	Actual Density, g/cm^3	Theoretical Density, %
70 (10)	2.16	57.75
103 (15)	2.20	58.82
138 (20)	2.25	60.16
172 (25)	2.27	60.7
206 (30)	2.30	61.5
276 (40)	2.31	61.7

Springback was about 2.5% at all pressures, which suggests that the binder system has a large working range. This is a sought-after binder property in industrial pressing applications. Final dimensions can be altered by changing the green density, which, in turn, can be altered by adjusting the pressing pressure.

7.3 Binder Removal

Earlier experience with AlN showed that it was possible to remove a similar binder in air. Figure 4 shows the weight-loss versus temperature curve for spray-dried AlN-Al_2O_3 mixtures. The weight loss recorded at 225°C signals the beginning of decomposition and removal of organics. For practical purposes, these processes are completed when temperatures reach 575°C. Note that there is no weight gain

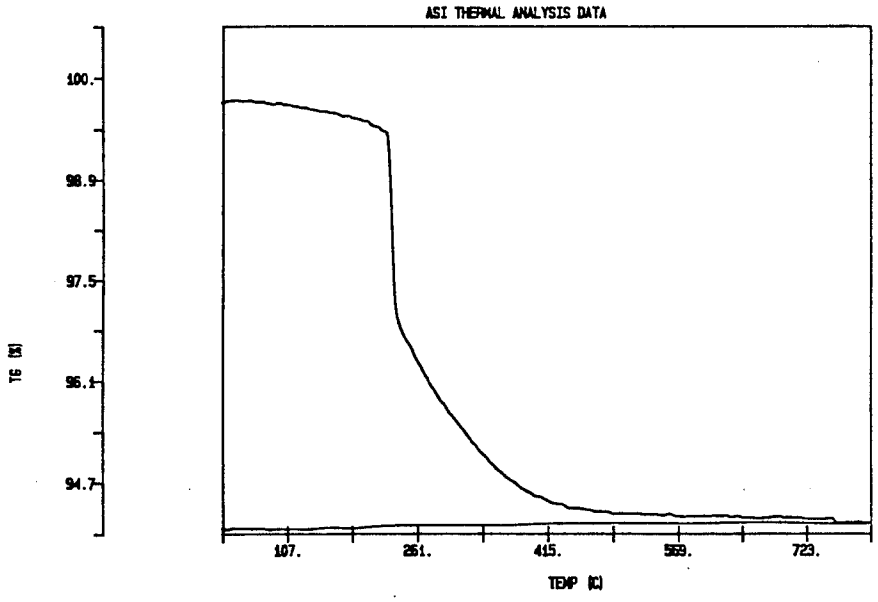

Figure 4. Thermal Gravimetric Analysis Curve Showing Binder Removal Behavior of Spray-Dried Powders in Air

at temperatures as high as 800°C, which suggests that AlN did not oxidize in air under experimental conditions. Based on thermal gravimetric analysis data, the following binder-removal conditions were defined and successfully used:

- Heating rate: 150°C/hr
- Temperature: 575°C
- Time at temperature: 2 hr
- Environment: Air

7.4 Sintering and Microstructural Evaluation

Sintered dimensions were measured, and shrinkages were calculated. Densities were measured by the liquid immersion technique. The results are tabulated in Table 5.

The results of the x-ray diffraction studies are given in Table 6. As predicted by the AlN-Al_2O_3 phase diagram, the samples are composed of AlN and AlON polytype phases. However, the presence of three phases in two phase regions suggests that either the AlN-Al_2O_3 phase diagram of McCauley and Corbin is inaccurate or a one-hour holding time was inadequate to reach phase equilibrium because of the possibly exothermic nature of the AlN-Al_2O_3 reactions. It is also possible that the different oxygen contents in starting AlN powders may be responsible for the observed discrepancy. We cannot substantiate this hypothesis, however, since McCauley and Corbin did not give the starting powder analysis in their work. A complete understanding of this issue is not within the scope of the Phase I study and should be pursued in Phase II.

As the reaction temperature or Al_2O_3 content increases, the weight loss increases. This behavior is attributed to the loss of Al_2O_3 by evaporation. Indeed, at 2100°C and above, all compositions except for E and F (the two with the highest AlN content) were heavily evaporated or molten. Excessive weight loss and shrinkage can cause problems such as dimensional control and cracking during sintering. Therefore, the sintering must be performed at lower temperature once the promising systems are identified.

Microstructures of all of the samples were initially evaluated under a light microscope to select the ones with fibrous microstructures for evaluation by SEM. It was not feasible to analyze all the microstructures by SEM in the Phase I program. Microstructures of compositions C, D, E, F, DY, EY, and DYS are given in Figures 5, 6, 7, 8, 9, 10, and 11, respectively.

Figures 5, 6, and 7 show the formation of acicular grains, which is expected to improve the mechanical properties of the base material. However, the mere presence of acicular grains does not guarantee higher strength and higher fracture toughness.

It is well known that ceramics with the same reinforcement can have very different properties depending on the reinforcement aspect ratio and reinforcement-matrix interface. It has been shown for several ceramic systems that increasing the diameter of the reinforcement increases the fracture toughness but reduces the strength of the material. The mere presence of elongated grains, in itself, does not guarantee a ceramic with improved mechanical properties. Toughening mechanisms such as crack deflection and pull-out and strengthening mechanisms such as load transfer depend upon the reinforcement-matrix interface. Weak interfaces promote crack deflection and pull-out, thereby increasing the fracture

Table 5. Experimental Results

Sample	Wg, g	Wf, g	Ws, g	Dg, mm	tg, mm	Df, mm	tf, mm	d, g/cm3	D, %	t, %	Wl, %
	RUN 1	**1900°C**	**1 hr**								
A19	1.1036	1.095	0.8491	16.5354	2.38	14.019	2.053	3.524573	15.21826	13.7395	0.779268
A25	1.0942	1.083	0.8407	16.5354	2.39	14.039	2.002	3.53774	15.09731	16.23431	1.023579
B4	1.1015	1.093	0.8449	16.5616	2.403	14.021	2.06	3.486939	15.34031	14.27382	0.771675
B6	1.1044	1.097	0.8496	16.5636	2.3663	14.073	2.038	3.509602	15.03659	13.87398	0.670047
C3	1.1077	1.1	0.8484	16.5223	2.381	14.116	2.054	3.460453	14.56395	13.73373	0.695134
C4	1.1134	1.107	0.8541	16.5223	2.392	14.114	2.056	3.464573	14.57606	14.04682	0.574816
D4	1.1121	1.105	0.8479	16.56	2.412	14.168	2.071	3.401818	14.44444	14.13765	0.638432
D9	1.1175	1.11	0.8524	16.561	2.431	14.148	2.099	3.410578	14.57038	13.65693	0.671141
E1	1.1145	1.107	0.822	16.564	2.582	14.323	2.263	3.074353	13.52934	12.35476	0.672948
E6	1.1273	1.12	0.8315	16.561	2.623	14.314	2.281	3.072721	13.56802	13.03851	0.647565
F7	1.1116	1.108	0.8181	16.565	2.758	14.095	2.367	3.025119	14.91096	14.17694	0.323858
F9	1.1102	1.106	0.8139	16.564	2.763	14.144	2.385	2.996915	14.61	13.68078	0.37831
G5	1.1144	1.106	0.8547	16.555	2.367	14.122	2.043	3.483482	14.69647	13.68821	0.753769
G10	1.1209	1.113	0.8603	16.559	2.379	14.154	2.052	3.486108	14.52382	13.74527	0.704791
	RUN 5	**1950°C**	**1 hr**								
A17	1.0901	1.0765	0.8372	16.5354	2.38	13.906	2.05	3.560592	15.90164	13.86555	1.247592
B10	1.0802	1.0674	0.8299	16.552	2.334	13.953	2.005	3.557251	15.70203	14.09597	1.184966
C18	1.1156	1.1027	0.854	16.561	2.388	14.02	2.059	3.509397	15.34328	13.77722	1.156328
D7	1.1237	1.11	0.8548	16.561	2.454	14.049	2.12	3.442653	15.16817	13.61043	1.219187
E11	1.1247	1.1085	0.812	15.564	2.615	14.563	2.322	2.959116	6.431509	11.20459	1.440384
F8	1.1132	1.0969	0.8017	16.565	2.769	14.333	2.414	2.941045	13.47419	12.82051	1.464247
G15	1.1271	1.1018	0.8565	16.553	2.38	13.958	2.055	3.555135	15.67692	13.65546	2.244699
	RUN 4	**2000°C**	**1 hr**								
A14	1.105	1.0729	0.836	16.5354	2.41	13.808	2.077	3.584636	16.49431	13.81743	2.904977
B15	1.1032	1.0779	0.8384	16.558	2.372	13.944	2.024	3.562246	15.78693	14.67116	2.293328
C10	1.1159	1.093	0.8481	16.554	2.395	13.953	2.068	3.532501	15.71221	13.65344	2.052155
D12	1.1242	1.0963	0.8464	16.556	2.433	13.983	2.092	3.472275	15.54119	14.01562	2.481765
E7	1.1099	1.0861	0.7959	16.562	2.582	14.482	2.285	2.962261	12.55887	11.50271	2.144337
F3	1.1291	1.106	0.8024	16.566	2.797	14.309	2.428	2.883396	13.62429	13.19271	2.045877
G9	1.1173	1.085	0.8446	16.553	2.374	13.962	2.044	3.572286	15.65275	13.90059	2.890898
	RUN 7	**2050°C**	**1 hr**								
E17	1.1196	1.0857	0.8016	16.566	2.607	14.316	2.297	3.02475	13.58204	11.89106	3.027867
F14	1.1215	1.006	0.8002	16.563	2.772	14.239	2.395	3.869043	14.03127	13.60029	10.29871
	RUN 6	**2050°C**	**1 hr**								
E4	1.1284	1.1024	0.8156	16.565	2.622	14.302	2.287	3.042363	13.66133	12.77651	2.304147
F11	1.1245	1.1014	0.8007	16.563	2.785	14.239	2.417	2.899096	14.03127	13.21364	2.054246
	RUN 3	**2100°C**	**1 hr**								
E2	1.1242	1.1237	0.8331	16.564	2.616	14.259	2.292	3.060594	13.91572	12.38532	0.044476
	RUN 2	**2200°C**	**1 hr**								
E3	1.1151	0.974	0.7251	16.564	2.598	14.077	2.28	3.097312	15.01449	12.24018	12.65357
F15	1.119	1.023	0.7421	16.564	2.771	14.285	2.434	2.882536	13.75875	12.16167	8.579088

Wg = green weight
Wf = sintered weight
Ws = submersed weight
Dg = green diameter
tg = green thickness
Df = sintered diameter
tf = sintered thickness
d = density
Wl = weight loss

Table 6. Phase Compositions of Sintered Samples

SAMPLE	TEMPERATURE					
	1900°C	1950°C	2000°C	2050°C	2100°C	2200°C
A	γ-AlON Al_3O_3N $Al_9O_3N_7$(27R)	γ-AlON Al_3O_3N $Al_9O_3N_7$(27R)	γ-AlON Al_3O_3N $Al_9O_3N_7$(27R)	γ-AlON Al_3O_3N $Al_9O_3N_7$(27R) SE	M, E	M, E
B	γ-AlON Al_3O_3N $Al_9O_3N_7$(27R)	γ-AlON Al_3O_3N $Al_9O_3N_7$(27R)	γ-AlON Al_3O_3N $Al_9O_3N_7$(27R)	SE	M, E	M, E
C	γ-AlON Al_3O_3N $Al_9O_3N_7$(27R)	NA	γ-AlON Al_3O_3N $Al_9O_3N_7$(27R)	γ-AlON Al_3O_3N $Al_9O_3N_7$(27R) $Al_6O_3N_4$(12H)	γ-AlON Al_3O_3N $Al_9O_3N_7$(27R) $Al_6O_3N_4$(12H)	M, E
D	γ-AlON Al_3O_3N $Al_9O_3N_7$(27R)	γ-AlON Al_3O_3N $Al_9O_3N_7$(27R)	γ-AlON Al_3O_3N $Al_9O_3N_7$(27R)	γ-AlON Al_3O_3N $Al_9O_3N_7$(27R) M, E	M, E	M, E
E	$Al_9O_3N_7$(27R) $Al_7O_3N_5$(21R) γ-AlON	$Al_9O_3N_7$(27R) $Al_7O_3N_5$(21R) γ-AlON	$Al_9O_3N_7$(27R) $Al_7O_3N_5$(21R) γ-AlON	$Al_9O_3N_7$(27R) $Al_7O_3N_5$(21R)	$Al_9O_3N_7$(27R) $Al_7O_3N_5$(21R)	$Al_9O_3N_7$(27R) $Al_7O_3N_5$(21R)
F	AlN γ-AlON	NA	$Al_9O_3N_7$(27R) AlN γ-AlON	NA	AlN $Al_9O_3N_7$(27R) γ-AlON	AlN $Al_9O_3N_7$(27R)
G	γ-AlON Al_3O_3N $Al_9O_3N_7$(27R)	γ-AlON Al_3O_3N $Al_9O_3N_7$(27R)	γ-AlON Al_3O_3N $Al_9O_3N_7$(27R)	γ-AlON Al_3O_3N $Al_9O_3N_7$(27R) Flaky	M, E	M, E

NA = not analyzed
M = molten
E = evaporated
SE = slight evaporation

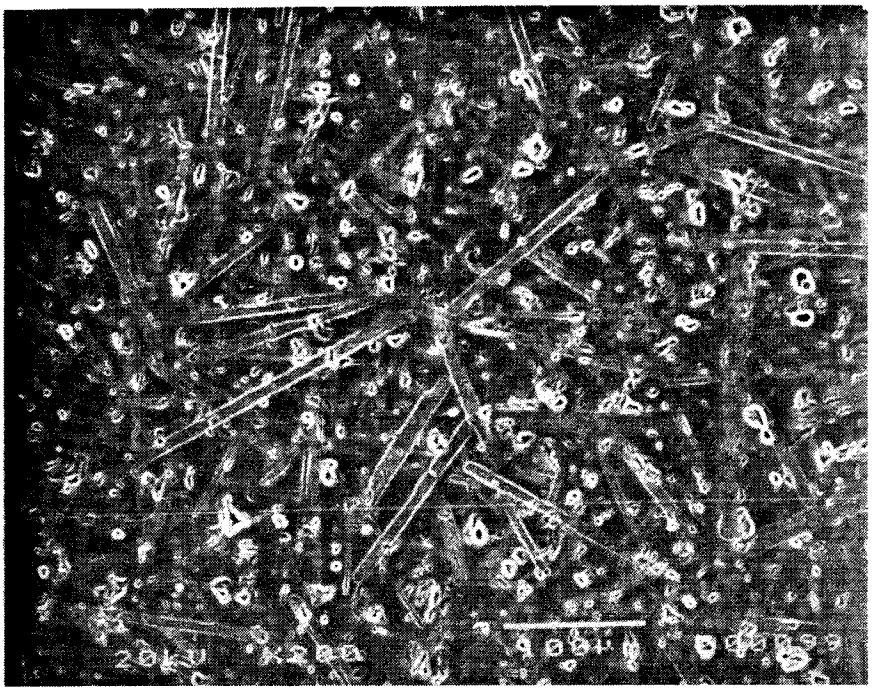

(a)

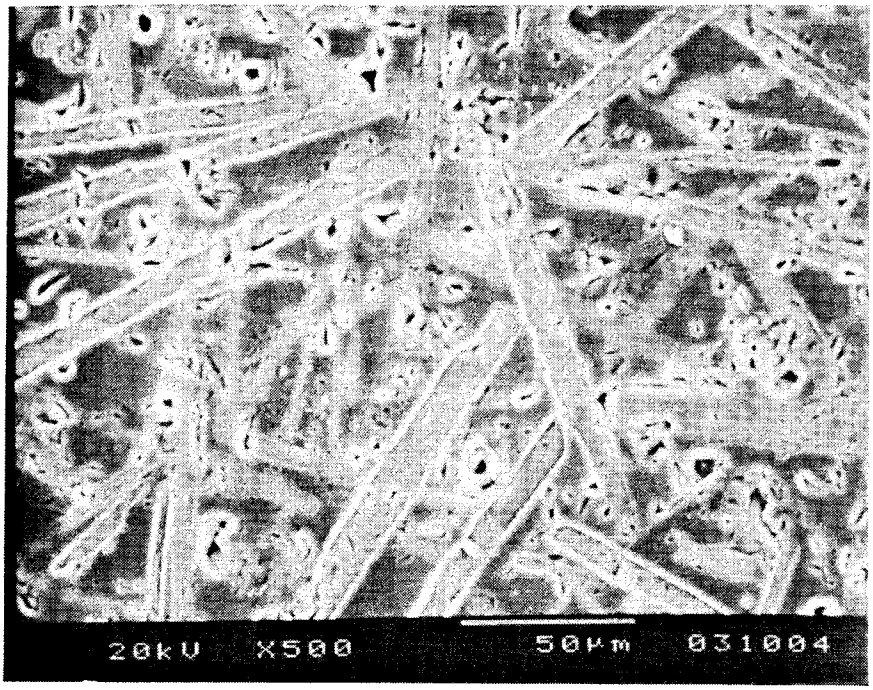

(b)

Figure 5. Microstructure of Composition C After Sintering at (a) 2050°C; (b) High Magnification of (a); and (c) 2100°C for 1 Hour

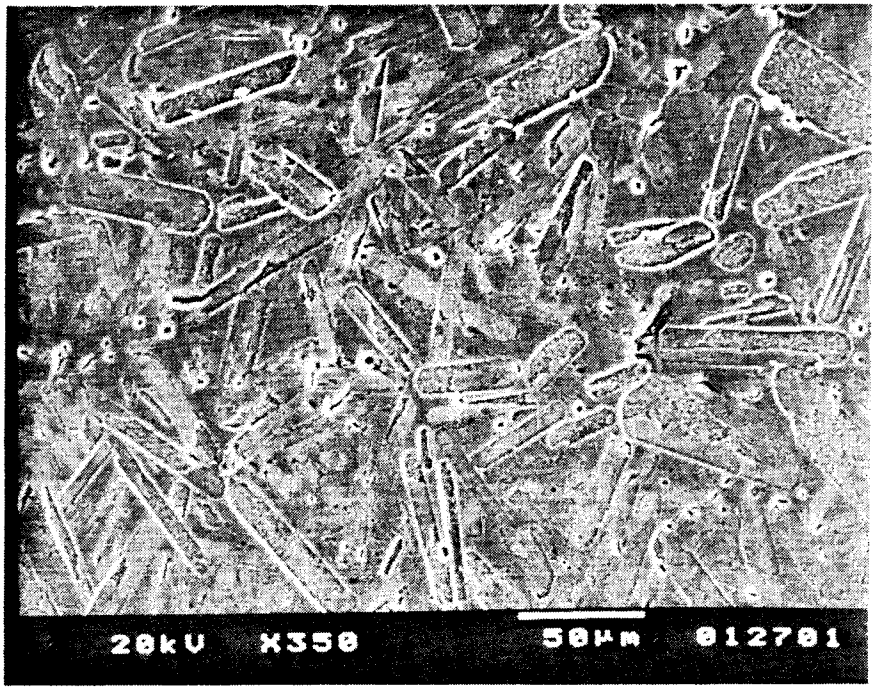

(c)

Figure 5. Microstructure of Composition C After Sintering at (a) 2050°C; (b) High Magnification of (a); and (c) 2100°C for 1 Hour (Cont.)

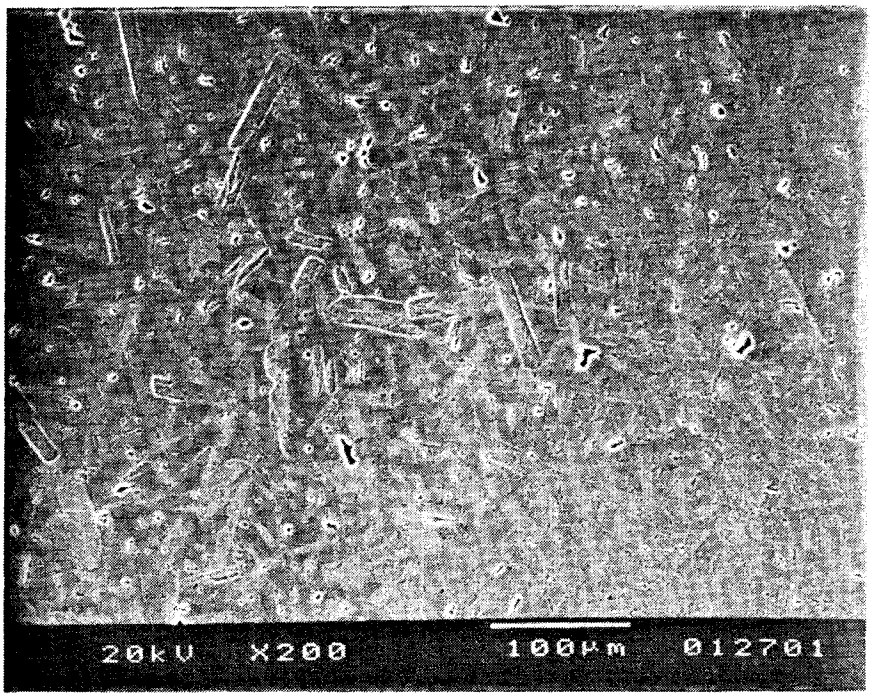

Figure 6. Microstructure of Composition D After Sintering at 2100°C for 1 Hour

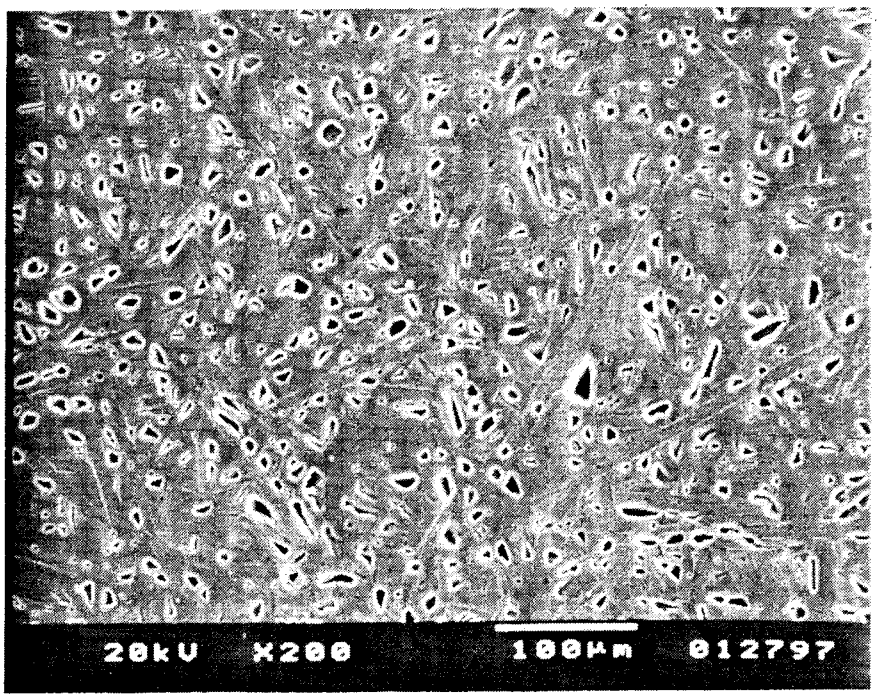

(a)

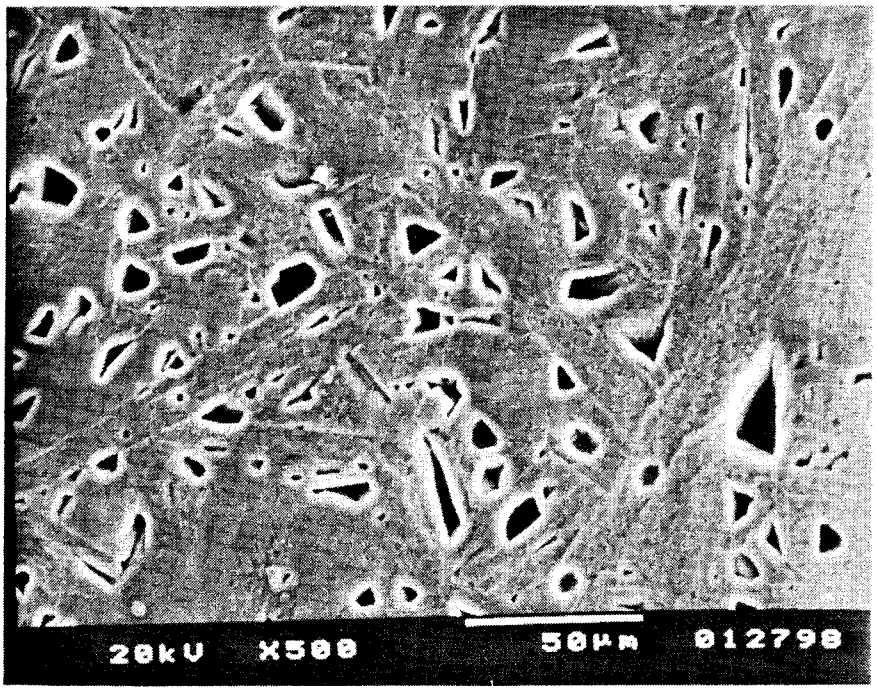

(b)

Figure 7. Microstructure of Composition E After Sintering at 2200°C for 1 Hour - (a) Low Magnification; (b) High Magnification

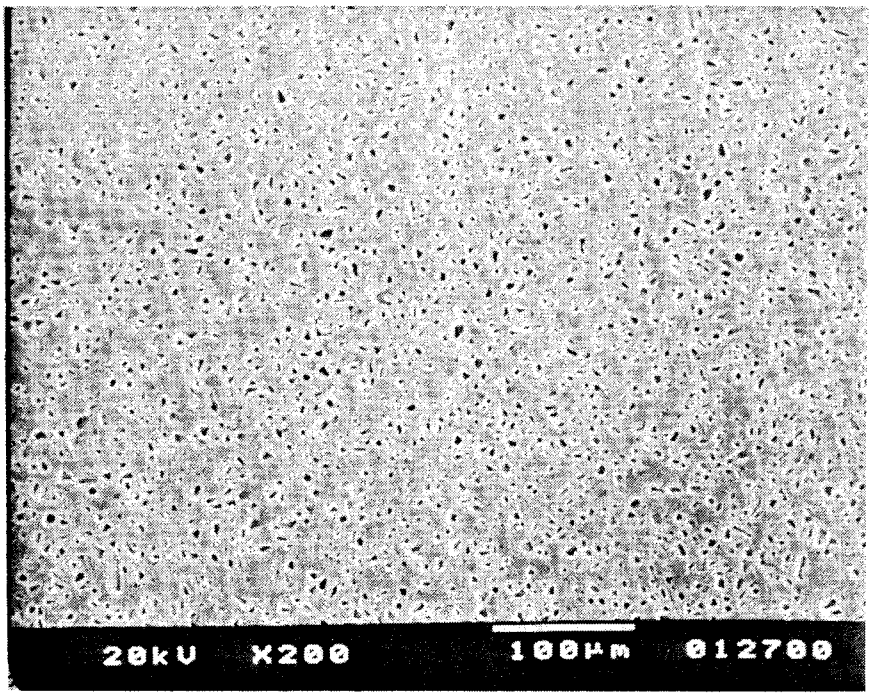

(a)

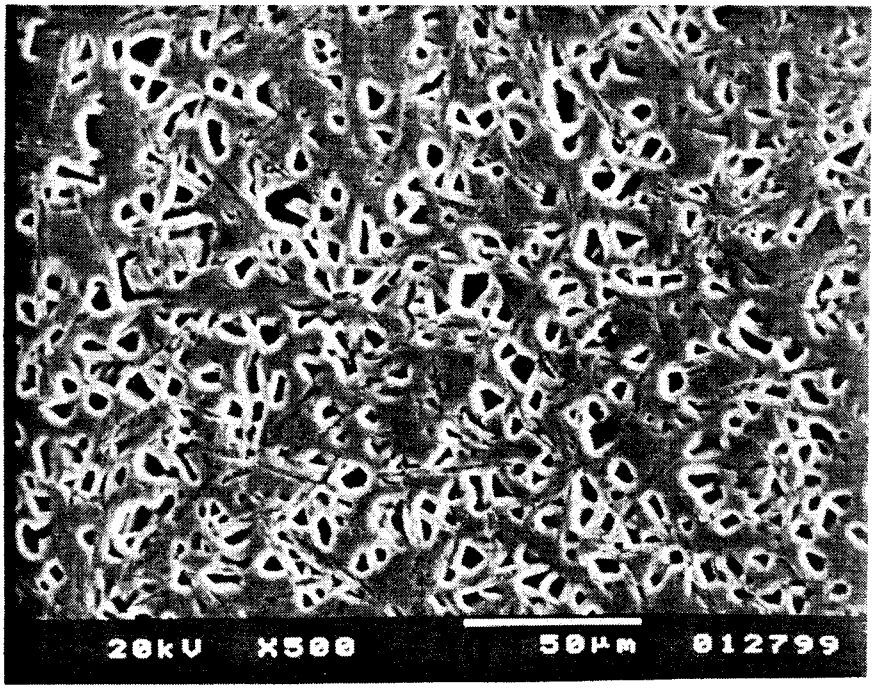

(b)

Figure 8. Microstructure of Composition F After Sintering at 2200°C for 1 Hour - (a) Low Magnification; (b) High Magnification

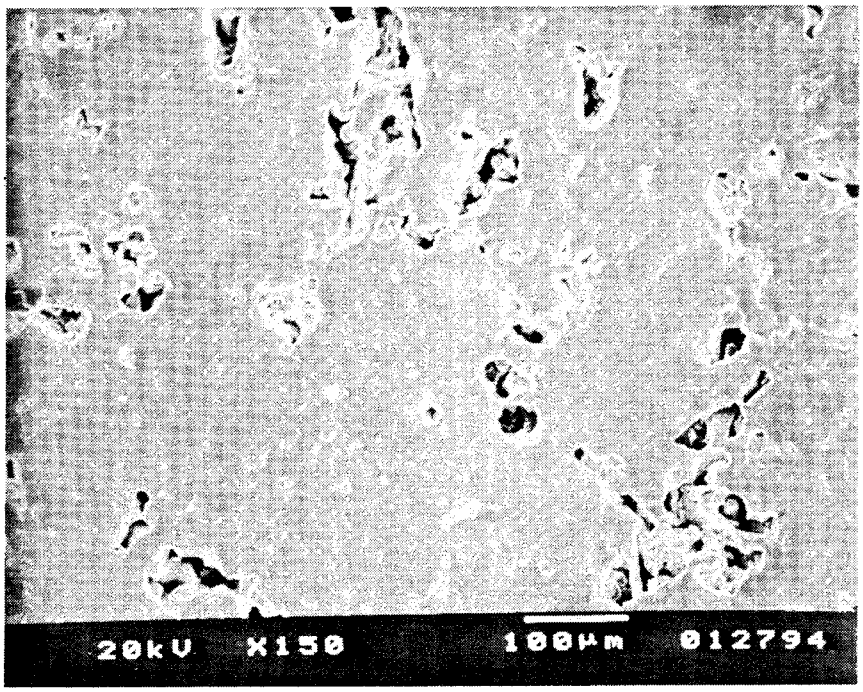

Figure 9. Microstructure of Composition DY After Sintering at 2000°C for 6 Hours

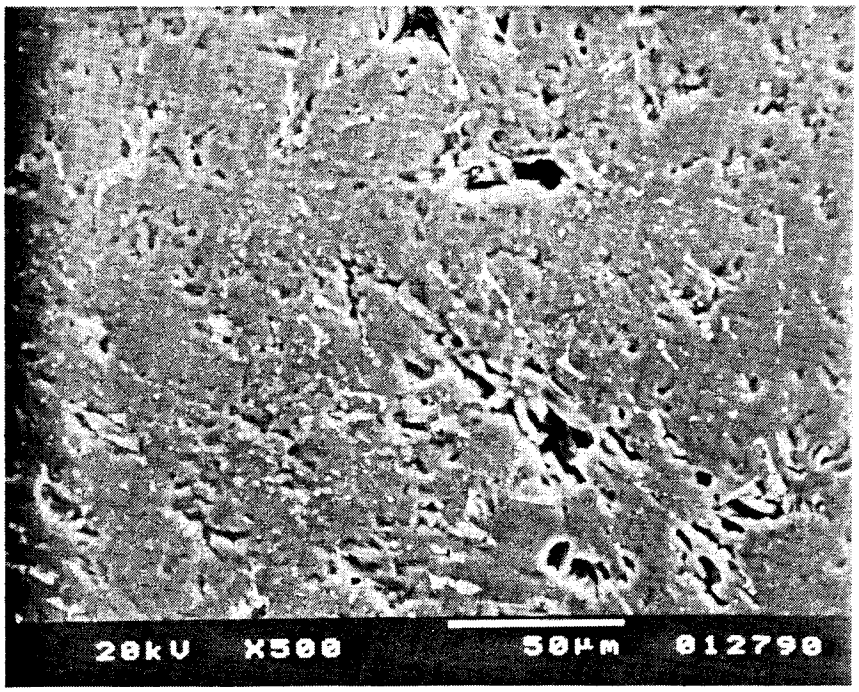

Figure 10. Microstructure of Composition EY After Sintering at 2000°C for 6 Hours

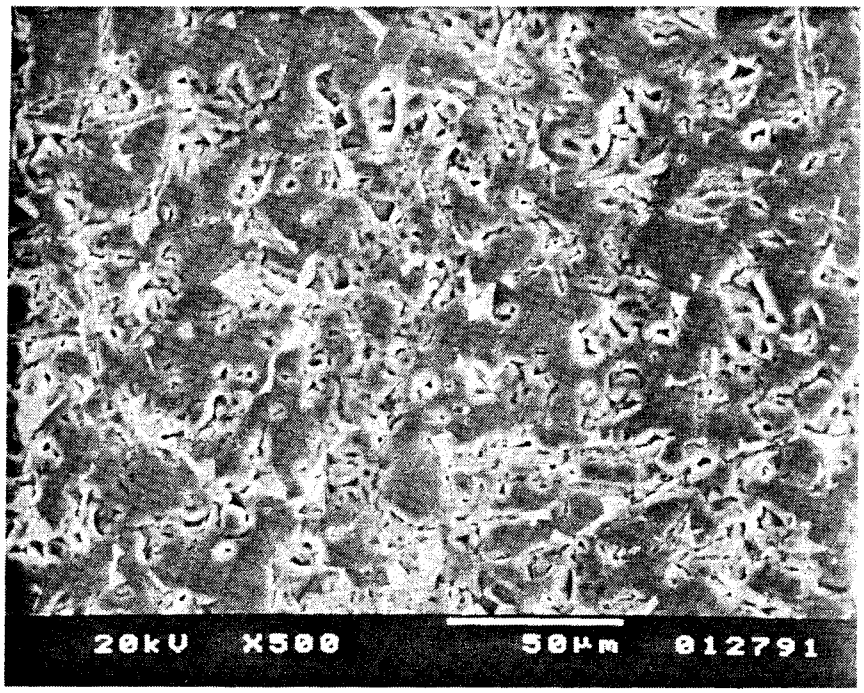

Figure 11. Microstructure of Composition DYS After Sintering at 1850°C for 6 Hours

toughness. But the interface should not be too weak, because it can degrade the strength by acting as a flaw origin. The nature of the interface is dictated by the chemical compositions of the matrix surrounding the reinforcement and of the reinforcement surface. The grain size, its distribution, and the aspect ratio of elongated grains are also important in improving mechanical properties. Therefore, once the elongated grain microstructure is achieved, it may be necessary to manipulate the microstructure to control the interface and enhance the properties of the composite.

It is also apparent from Figures 5 through 7 that acicular grain growth is accompanied by excessive grain growth, which is a common phenomenon in the AlN-Al_2O_3 system. The reason for this excessive grain growth is not known, but it is speculated that it is associated with the AlN-Al_2O_3 reaction to form AlON (Savrun, 1994).

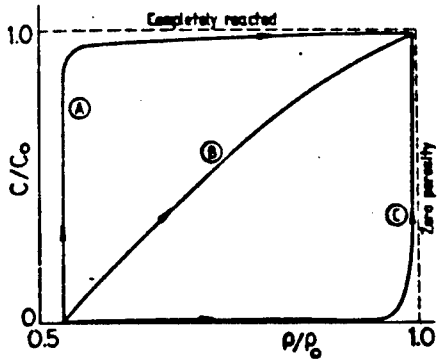

Figure 12. Processing Paths for Reaction Sintering - ρ_0 Is the Theoretical Density of the Product (Yanyun and Brooks, 1985)

When the rate of reaction is much higher that the pore-removal rate [see curve (A) in Figure 12], the reaction is well advanced before densification can be observed. With such a reaction/densification sequence, the grain growth of the AlON that has already formed is difficult to control. Consequently, the pores may be trapped in large AlON grains, making further densification difficult. Pore removal is difficult because it is controlled by slow lattice diffusion.

Curve (C) shows the processing path of a reaction sintering where the reaction rate is much lower than that of pore removal. Pore removal occurs before the reaction begins, allowing AlON formation to take place in a fully dense microstructure. It is therefore possible to control conditions and prevent pore trapping in AlON grains. Curve (B) represents the behavior of a system in which the reaction and densification rates are of comparable magnitude. Our objective will be to choose the processing conditions that favor a sintering path similar to curve (C) in Phase II.

It is well known in ceramics that, as the grain size increases, the strength decreases, since large grains can act as flaws. Therefore, the gain in strength by the acicular grains may be offset by the large grains and porosity (please see next section for complete discussion).

Figure 8 shows the microstructure of a 95% AlN - 5% Al_2O_3 composition after sintering at 2200°C. The microstructure was the most porous of all microstructures. This is expected because of the high concentration of AlN. There is also a lack of acicular grains in the microstructure; this observation is in contrast to that of Krishnan et al. (1986), who observed the formation of acicular grains after sintering at 2200°C for 1 hour. Since the acicular grains are formed by oxygen insertion into the AlN lattice, the amount of available oxygen, i.e., in the raw AlN, may be responsible for the observed difference. However, this cannot be substantiated, because Krishnan et al. (1986) do not give the starting powder compositions.

Figures 9 and 10 show the effects of the addition of 4% wt Y_2O_3 on the microstructures of compositions D and E. Porosity is apparent in both microstructures. This is attributed to the evaporation of the yttrium aluminate phase due to high sintering temperatures (2000°C). Another feature that can be seen in both Figures 9 and 10 is the lack of acicular grains. At this point, we cannot offer any explanation, since the same compositions without the addition of Y_2O_3 at similar temperatures gave microstructures with acicular grains. We can hypothesize that Y_2O_3 reacts with Al_2O_3 to form Y_2O_3-Al_2O_3, which then evaporates and leaves very little oxygen available to create acicular grains. However, this hypothesis should be checked.

The addition of SiO_2 appears to suppress evaporation by the liquid phase which is against intuition. However, if we consider that the sintering temperature is 1850°C—200°C lower than the composition without SiO_2—the observation becomes plausible.

From Figures 5 through 11, it is apparent that acicular grain formation increases with increasing temperature. It is possible that oxygen diffuses in while nitrogen diffuses out from the AlN lattice during acicular grain formation. Energy dispersive x-ray spectroscopy supports this hypothesis, as shown in Figure 13. However, it should not be taken as the only explanation, because we have detected oxygen both on equiaxed and acicular grains. A more detailed structural analysis, such as transmission electron microscopy and electron energy loss spectroscopy, is necessary to understand the acicular grain formation.

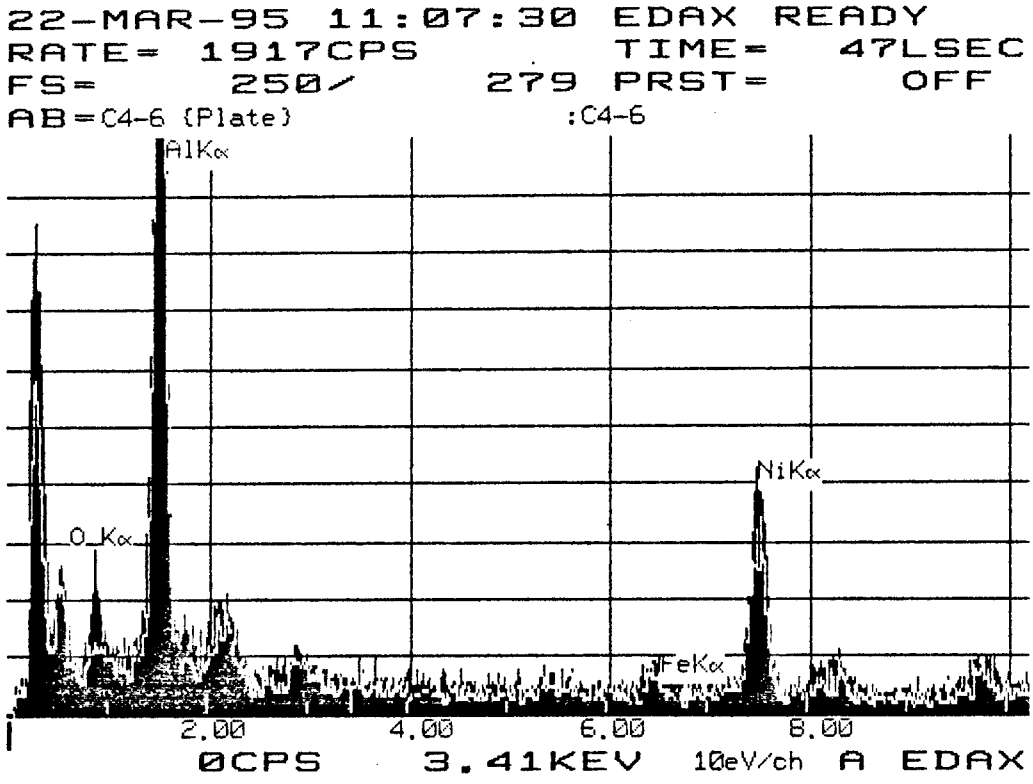

Figure 13. EDS Spectrograph of Acicular and Equiaxed Grains

The presence of large grains and intragranular porosity in all microstructures suggests that grain growth is faster than densification. Sintering may be viewed as a competition between densification and grain growth or coarsening. While both processes lead to a reduction in the free energy of a sintering body, the grain growth is detrimental to the achievement of high density because it leads to a reduction in the driving force of the densification process. Therefore, it must be minimized. There are several ways the problem can be approached:

- By employing a stepwise sintering in which the first step is to densify Al_2O_3 at a temperature (i.e., 1500°C) that is lower than the AlN-Al_2O_3 reaction temperature (about 1700°C). However, the effect of stepwise sintering on acicular grain formation must be clarified, since it may hinder acicular grain growth by slowing down the kinetics of the process. The kinetics is controlled by a solid-state diffusion mechanism in which N^{3-} and O^{2-} ions are the rate-controlling species.
- By decreasing the grain-boundary mobility through the use of suitable dopants such as magnesia (MgO). MgO may be precipitated at the grain boundaries, and its pinning action may slow the grain growth. To accomplish this, however, the solubility limit for MgO in the AlN-Al_2O_3 reaction product, AlON, at the sintering temperature must be determined.
- By employing a transient liquid phase sintering. Diffusion of the rate-controlling species can be accelerated in the liquid phase, which can then be eliminated by evaporation or by dissolution in the solid phase. This approach has been shown to work in the AlN-Y_2O_3-SiO_2 system (Komeya et al., 1974).

7.5 Mechanical Testing

The strength values and Weibull parameters are given in Table 7. Aluminum nitride is included for comparison purposes.

Table 7. Weibull Parameters for Strength Distributions

Composition	No. of Specimens	σ_{avg}, MPa	Range, MPa	σ_0	*m*	*R*
C	10	337 ∓ 87	247-550	372.5	3.95	0.91
D	10	320 ∓ 41	243-391	339.6	7.43	0.99
DY	10	238 ∓ 26	202-287	250.0	9.02	0.97
DYS	10	110 ∓ 8	102-128	113.0	11.11	0.85
AlN	19	350 ∓ 57	253-450	374.0	6.50	0.98

The presence of elongated grains increases the strength of compositions C and D. However, the strength values are not any better that that of AlN. This can be attributed to the excessive grain growth and the large porosity as shown in Figures 4 and 5. The wide strength range observed in composition C is evident by the lowest Weibull modulus. Furthermore, the high strengths (up to 550 MPa) observed in this group suggest that there is a potential for higher strengths once the microstructure is optimized, that is, excessive grain growth and porosity are eliminated. The addition of Y_2O_3 (composition DY) and (Y_2O_3+SiO_2) appears to weaken the material, as evidenced by the lower average strengths. The relatively tight strength distribution as reflected in the higher Weibull modulus values suggests that a single

flaw population is responsible for the observed low strengths. If we consider the microstructures observed in these compositions (Figures 8 and 9), we see that large pores are responsible for the low strengths. We believe the porosity exists due to evaporation of yttria- and silica-containing liquid phases at high sintering temperatures. The observed high correlation coefficients, *R*, suggest a very good fit of the data to the two-parameter Weibull model, with the exception of composition DYS.

Hardness, elastic modulus, and fracture toughness values of the compositions investigated are given in Table 8. AlN and Al_2O_3 are also included for comparison purposes.

Table 8. Hardness, Elastic Modulus, and Fracture Toughness Data

Composition	Hardness, GPa	Elastic Modulus, GPa	Fracture Toughness, MPa·m$^{1/2}$
C	15.24	266	3.09
D	14.73	278	2.50
DY	14.69	274	2.39
DYS	14.51	206.5	1.81
AlN	12.00	320	2.90
Al_2O_3	19.00	370	2.50

All compositions displayed higher hardness values than end-member AlN; however, the hardness values were lower than the other end-member Al_2O_3. This behavior is expected and has also been observed in AlON systems. However, the elastic modulus values were lower than those for both end-members. This can be attributed to the high porosity present in the test samples.

In agreement with strength measurements, composition C has the highest fracture toughness, but it is well below the target value of 8 to 10 MPa·m$^{1/2}$. This behavior can be attributed to the excessive grain growth in compositions C and D. The addition of Y_2O_3 and SiO_2 (composition DYS) causes a decrease in the fracture toughness of composition D. This behavior is attributed to the presence of glassy phases in the DYS composition.

8. CONCLUSIONS

- Self-reinforced microstructures containing acicular grains can be synthesized.
- Rapid grain growth is observed. X-ray diffraction of phase evaluation and observations on the evolution of microstructures suggest that the reaction rate between AlN and Al_2O_3 and the coarsening rate are faster than the densification rate. This behavior causes incomplete densification.
- Some improvement in the strength and fracture toughness can be achieved; however, the improvement appears to be offset by the excessive grain growth and porosity.
- The addition of liquid-phase formers Y_2O_3 (4% wt) and SiO_2 (1% wt) suppresses acicular grain formation at 1850°C, while at 2100°C the liquid phase evaporates and leaves porosity in the material.

9. RECOMMENDATIONS

- Only with an understanding of the acicular grain formation mechanism and of the physical and chemical nature of the interface can the self-reinforced microstructure be controlled and modified. Therefore, the critical parameters of starting-powder chemistry, sintering-aid amount, silica content, and sintering conditions should be investigated further to control the microstructures, in particular the grain growth, the grain morphology, the aspect ratio, and the nature of the interface between elongated and equiaxed grains.
- Reaction rates and densification rates should be determined and compared to each other. An attempt, then, should be made to adjust the reaction and/or sintering rates, i.e., by adjusting particle size. Since reaction and sintering rates are dependent on particle size, the relationship between them should be established.
- To improve the mechanical properties, the grain growth and excessive porosity must be eliminated. To do so, the sintering temperature must be reduced.
- Diffusion coefficients for oxygen in aluminum nitride, for nitrogen in alumina, and for both oxygen and nitrogen in aluminum oxynitride should be determined. This information is necessary to understand the excessive grain growth in the aluminum nitride-alumina system. Sintering mechanisms should be established.
- Stepwise sintering should be studied. An attempt should be made to sinter the major component Al_2O_3 before the AlN-Al_2O_3 reaction takes place. However, the effect of this approach on the acicular grain formation should be clarified.
- Sintering aids appear to be necessary to reduce the sintering temperature. A reduced sintering temperature may lead to a more economical process and to the development of a fine-grained material with increased strength and fracture toughness.
- The addition of MgO just above its solubility limits in the AlN-Al_2O_3 system should be studied. It is possible that MgO can precipitate at the grain boundaries and slow them down by a pinning action, thus, slowing down the grain growth. The process should be monitored by transmission electron microscopy.
- Reactive liquid-phase sintering should also be addressed. Y_2O_3 may be a good sintering aid since it does not affect the thermodynamics and kinetics of the AlN-Al_2O_3 reaction. The role of sintering aids, including Y_2O_3 and SiO_2, on the microstructural development, and particularly on acicular grain formation, must be clarified further, however, before using them as sintering aids.

REFERENCES

Anstis, G. R., Chantikul, P., Lawn, B. R., and Marshall, D. B. (1981) "A Critical Evaluation of Indentation Techniques for Measuring Fracture Toughness: I, Direct Crack Measurements," *J. Am. Ceram. Soc.*, Vol. 64, p. 533.

Corbin, N. D. (1989) "Aluminum Oxynitride Spinel: A Review," *J. Europ. Cer. Soc.*, Vol. 5, p. 143.

Jack, K. H. (1976) "Review: Sialons and Related-Nitrogen Ceramics," *J. Mater. Sci.*, Vol. 11, p. 1135.

Komeya, K., and Inoue, H. (1971) "The Influence of Fibrous Aluminum Nitride on the Strength of Sintered AlN-Y_2O_3," *Trans. J. Brit. Ceram. Soc.*, Vol. 70, p. 107.

Komeya, K., Inoue, H., and Tsuge, A. (1974) "Role of Y_2O_3 and SiO_2 Additions on the Sintering of AlN," *J. Am. Ceram. Soc.*, Vol. 57, p. 411.

Krishnan, K., et al. (1986) "Characterization of Long Period Polytypoid Structures in the Alumina-Aluminum Nitride System," *MRS Symp. Proc.*, Vol. 60, p. 211.

Lejus, A. M. (1964) "Sur la Formation à Haute Temperature de Spinelles Non-Stoetechiométriques et de Phase Derivées," *Rev. Hautes. Temp. et Refrac.*, Vol. 1, p. 53.

Long, G., and Foster, L. M. (1961) "Crystal Phases in the System Al_2O_3-AlN," *J. Am. Ceram. Soc.*, Vol. 44, p. 255.

McCauley, J. W., and Corbin, N. D. (1983) "High Temperature Reactions and Microstructures in the Al_2O_3-AlN System," *Progress in Nitrogen Ceramics*, Ed. F. L. Riley, Martinus Nijhoff, Boston, p. 111.

McCauley, J. W., et al. (1987) "Anion Controlled Microstructures in the Al_2O_3-AlN System," *Ceramic Microstructures 86*, Eds. J. A. Pask and A. G. Evancs, p. 577, Plenum Press, New York.

Sarikaya, M., and Thomas, G. (1984) "New Studies in AlN Polytypoids," *Electron Microscopy*, Eds. A. Csadany et al., Vol. 1, p. 227.

Sarikaya, M., Aksay, I. A., and Thomas, G. (1985) "High Resolution Electron Microscopic Characterization of Interfaces in Ceramics," *Materials Science Research*, Vol. 9, p. 167.

Savrun, E. (1986) Ph.D. Thesis, University of Washington, Seattle, Washington.

Savrun, E. (1994) "Pressureless Sintered Aluminum Oxynitride for Transparent Armor Applications," QUEST TR-608, ARPA Contact No. DAAL04-92-C-0025.

Tkachenko, Y. G., et al. (1992) "Self-Reinforced Materials Based on Aluminum Nitride," *Porosh. Metall.*, Vol. 357, p. 69.

Yanyun, S., and Brooks, R. (1985) "Reaction Sintering,"*Sci. Sintering*, Vol. 17, p. 35.

Zangvil, A., and Doser, R. W. (1982) "Transmission Electron Microscopy of Al_2O_3-AlN Samples," Final Report for AMMRC, Contract No. DAAG46-81-M1377, August.

DISTRIBUTION LIST

ADDRESSEE	DODADD CODE	NUMBEROF COPIES
Program Officer ATTN: Steven Fishman, ONR 331 Office of Naval Research 800 North Quinch Street Arlington, VA 22217-5660	N00014	1
Administrative Contracting Officer DCMAO Seattle ATTN: Geg Seward Corporate Campus East III 3009 112th Ave. N.E. Seattle, WA 98004-8019	S4801A	1
Director, Naval Research Laboratory ATTN: Code 2627 Washington, D.C. 20375-5326	N00173	1
Defense Technical Information Center Bldg. 5, Cameron Station Alexandria, Virginia 22304-6145	S47031	2
Ballistic Missile Defense Organization ATTN: T/IS The Pentagon Washington, D.C. 20301-7100	HQ0006	1